The Reaction Mechanism for CD38. A Single Intermediate Is Responsible for Cyclization, Hydrolysis, and Base-Exchange Chemistries†

Anthony A. Sauve,‡ Cyrus Munshi,§ Hon Cheung Lee,§ and Vern L. Schramm*,‡

Department of Biochemistry, Albert Einstein College of Medicine, Bronx, New York 10461, and Department of Physiology, University of Minnesota, Minneapolis, Minnesota 55455

Received May 27, 1998

ABSTRACT: Human recombinant CD38 catalyzes the formation of both cyclic ADP-ribose and ADP-ribose products from NAD^+ and hydrolyzes cyclic ADP-ribose to ADP-ribose. The corresponding GDP products are formed from NGD^+. The enzyme was characterized by substrate and inhibition kinetics, exchange studies, rapid-quench reactions, and stopped-flow-fluorescence spectroscopy to establish the reaction mechanism and energetics for individual steps. Noncyclizable substrates NMN^+ and nicotinamide-7-deaza-hypoxanthine dinucleotide (7-deaza NHD^+) were rapidly hydrolyzed by the enzyme. The k_{cat} for NMN^+ was 5-fold higher than that of NAD^+ and has the greatest reported k_{cat} of any substrate for CD38. 7-deaza-NHD^+ was hydrolyzed at approximately one-third the rate of NHD^+ but does not form a cyclic product. These results establish that a cyclic intermediate is not required for substrate hydrolysis. The ratio of methanolysis to hydrolysis for cADPR and NAD^+ catalyzed by CD38 increases linearly with MeOH concentration. Both reactions produce predominantly the β-methoxy riboside compound, with a relative nucleophilicity of MeOH to H_2O of 11. These results indicate the existence of a stabilized cationic intermediate for all observed chemistries in the active site of CD38. The partitioning of this intermediate between cyclization, hydrolysis, and nicotinamide-exchange unites the mechanisms of CD38 chemistries. Steady-state and pre-steady-state parameters for the partition and exchange mechanisms allowed full characterization of the reaction coordinate. Stopped-flow methods indicate a burst of cGDPR formation followed by the steady-state reaction rate. A lag phase, which was NGD^+ concentration dependent, was also observed. The burst size indicates that the dimeric enzyme has a single catalytic site formed by two subunits. Pre-steady-state quench experiments did not detect covalent intermediates. Nicotinamide hydrolysis of NGD^+ precedes cyclization and the chemical quench decomposes the enzyme-bound species to a mixture of cyclic and hydrolysis products. The time dependence of this ratio indicated that nicotinamide bond-breakage occurs 4 times faster than the conversion of the intermediate to products. Product release is the overall rate-limiting step for enzyme reaction with NGD^+.

Human CD38 is a glycoprotein expressed during early and late stage maturation in the plasma membrane of β cells (*1*−*4*). Reports link its presence to cytokine-induced differentiation (*1*, *5*−*7*), cell adhesion (*1*, *6*, *8*) and signal transduction (*5*−*13*). A catalytic function in vivo has been proposed from the high sequence homology (68%) between CD38 and ADP-ribosyl-cyclase[1] (*14*). ADP-ribosyl cyclase converts NAD^+ to cyclic ADP-ribose (cADPR) (*15*, *16*). cADPR is a potent agonist of calcium release from intracellular Ca^{2+} stores and acts as a second messenger in a signal cascade from NO synthesis to the release of calcium caused by cADPR binding to ryanodine receptors (*1*, *16*−*22*). Both ADP-ribosyl cyclase and CD38 possess NAD^+ cyclase activity (*11*). CD38 has been implicated in the regulation of cADPR levels in mammalian cells (*20*−*22*). Moreover, cADPR appears to increase Ca^{2+} levels in specific cell types (*20*−*22*). The wide distribution of CD38 in brain (*20*−*24*), white blood cells (*2*), pancreas (*25*), and a variety of other tissues (*4*, *26*, *27*) suggests that this molecule may have a general signaling role via cADPR production in vivo.

The crystal structure of unliganded ADP-ribosyl cyclase from *Aplysia* reveals a homo-dimer (*28*). Each subunit possesses a cleft capable of accommodating NAD^+. In the cavity between the subunits a dinucleotide can be modeled in the geometry for intramolecular cyclization. It has been suggested that CD38 is a dimer with one active site for cADPR formation and a second for cADPR hydrolysis (*28*). Recombinant CD38 lacking the membrane-anchoring N-terminal domain has shown that the enzymatic activity of CD38 resides wholly in the cloned ecto-cellular domain (*29*, *30*). The availability of recombinant CD38 facilitates the determination of the reaction mechanism.

† This work was supported by NIH Postdoctoral Fellowship GM19335 and Research Grant AI34342 from the NIH.

* To whom correspondence should be addressed: Department of Biochemistry, Albert Einstein College of Medicine, Bronx, NY 10461. Telephone: (718) 430-2813. FAX: (718) 430-8565. E-mail: vern@aecom.yu.edu.

‡ Albert Einstein College of Medicine.

§ University of Minnesota.

[1] Abbreviations: ADP-ribosyl, adenosine diphosphate-ribosyl; ADPR, adenosine diphosphate-ribose; cADPR, cyclic adenosine diphosphate-ribose; GDPR, guanosine diphosphate-ribose, cGDPR, cyclic guanosine diphosphate-ribose; NAD^+, nicotinamide diphosphate-ribose (oxidized form); NMN^+, nicotinamide mononucleotide; NGD^+, nicotinamide-guanine dinucleotide; NHD^+, nicotinamide-hypoxanthine dinucleotide; 7-deaza-NHD^+, nicotinamide-7-deaza-hypoxanthine dinucleotide; TFA, trifluoroacetic acid; TCA, trichloroacetic acid.

S0006-2960(98)01248-3 CCC: $15.00 © 1998 American Chemical Society
Published on Web 08/29/1998

Two mechanisms have been proposed to explain the reactivity of NAD^+ and other dinucleotides with CD38 (*11*, *31*−*35*). One mechanism proposes an obligatory cyclization of NAD^+ to cADPR followed by hydrolysis to ADP-ribose (ADPR) (*11*). The second proposal is based on the mechanism of spleen NAD^+ glycohydrolases which also function as NAD^+ and NGD^+ cyclases and hydrolases (*32*−*35*). The mechanism of NAD^+ glycohydrolases and that suggested for CD38 proposes that all products are derived from a single intermediate that partitions to the cyclic or hydrolytic products. The present work resolves these views of the enzymatic mechanism of CD38. Spectroscopic, chemical reactivity, kinetic, and rapid quench studies are presented to furnish a complete microscopic analysis of the catalytic and rate steps for CD38.

METHODS AND MATERIALS

General Experimental. Solvents, compounds, and enzymes were used as obtained from commercial vendors unless otherwise indicated. Adenosine kinase was purified from beef liver (*36*). The stopped-flow spectrophotometer was an Applied Photophysics Model SX 17MV interfaced to an Acorn computer processing system using AP software. The rapid-quench instrument was a Kintek Model RQF-3 fitted with eight variable volume loops. HPLC used a Hitachi L-6200 combined with a digital variable wavelength LINEAR UVIS 204 detector set to 260 nm and a Hitachi D-2000 recorder/integrator. Recombinant CD38 was made and purified according to published procedures (*30*).

Synthesis of 5′-Phospho-7-deaza-inosine. To a suspension of 2.0 mg (7.5 μmol) of tubercidin in 1.5 mL of 50 mM K_2PO_4 at pH 7.5 was added 50 μL of adenosine deaminase (calf intestine, 10 mg/mL) obtained from Boehringer Mannheim. The reaction was incubated at 37 °C for 12 h after which an additional 50 μL of enzyme was added. Progress of the reaction to the product 7-deaza-inosine was monitored by HPLC using a C-18 Waters Bondapak column (2.5 mm × 100 mm) eluted with: 2 mL/min 96:4 A/B (A, 50 mM ammonium acetate, pH 5.0; B, 50% H_2O, 50% MeOH). The retention times were 24.0 min for tubercidin and 19 min for 7-deaza-inosine. After conversion in excess of 98%, the reaction was terminated by heating for 1 min at 110 °C and spinning for 2 min by tabletop centrifugation (12 000 min^{-1}) to pellet protein. To the decanted supernatant was added an equal volume of 100 mM PIPES pH 6.5 buffer containing 2 mM ATP, 10 mM phosphoenol pyruvate, 100 mM KCl, and 10 mM $MgCl_2$. Adenosine kinase and pyruvate kinase (0.5 unit each) were added to start the reaction. The reaction was incubated at 37 °C for 3.5 h until the reaction was in excess of 90% complete as determined by HPLC (see below). The product 5′-phospho-7-deaza-inosine was purified on a Waters C-18 Bondapak column using an ion-pairing solvent system 85:15 A/B (A, 100 mM triethylammonium acetate, pH 6.0; B, 50% MeOH, 50% H_2O) with an elution time of 5.0 min. The phosphate compound was lyophilized and repurified by HPLC elution 95:5 A/B (A, 0.1% TFA; B, 50% MeOH, 50% H_2O) and lyophilized. Treatment of this product with alkaline phosphatase rapidly regenerated the 7-deaza-inosine.

Synthesis of 7-Deaza-nicotinamide Hypoxanthine Dinucleotide. The monophosphate was coupled to repurified NMN^+ (Sigma, TFA conditions for repurification as described above) by a known procedure (*37*, *38*). The 7-deaza nucleotide and NMN^+ in respective amounts 2.5 μmol and 5 μmol and 60 μmol of $MgCl_2$ in 100 μL of distilled H_2O were evaporated by tabletop spin evaporator to dryness; 100 μL of 1.5 M HEPES−NaOH and 100 μL 5 M of 1-(3-dimethylaminopropyl)-3-ethylcarbodiimide hydrochloride (EDC) were added to the dried residue to initiate the coupling reaction. Incubation (15 h) at 37 °C was followed by dilution with 1.0 mL of water. The reaction mixture was purified by injection of 500 μL onto a Waters C-18 Bondapak column 2.5 mm × 100 mm using elution of 95:5 A/B (A, 100 mM triethylammonium acetate, pH 6.0; B, 50% MeOH, 50% H_2O). Lyophilization of the collected fractions afforded a 46% yield of 7-deaza-NHD^+. Chemical hydrolysis at 80 °C of this compound yielded nicotinamide and a second compound assigned to 7-deaza-inosine diphosphate-ribose. Cleavage of the diphosphate bond of 7-deaza-NHD^+ with snake venom diesterase provided NMN^+ and 5′-phospho-7-deaza-inosine (*38*).

Synthesis of [1′-^{3}H]NGD$^+$ and [8-^{3}H,carbonyl-^{14}C]NGD$^+$. [1′-^{3}H]NAD^+ was prepared as reported (*39*) and was treated with snake venom diesterase to obtain [1′-^{3}H]NMN^+ (*39*). The reaction mixture was heated to 110 °C for 40 s and spun to pellet protein; the supernatant was injected onto a C-18 column and eluted with 98:2 A/B (A, 0.1% TFA; B, 50% MeOH, 50% H_2O). The peak containing [1′-^{3}H]NMN^+ was collected and lyophilized. The [1′-^{3}H]NMN^+ residue was diluted to a concentration of 2 mM with 50 mM potassium phosphate pH 7.5 containing 5 mM $MgCl_2$ and 4 mM GTP. To this solution was added 1.0 unit of NAD^+ pyrophosphorylase and 0.1 unit of inorganic pyrophosphatase. The reaction was incubated at 37 °C and after 6 h 1.0 unit of NAD^+ pyrophosphorylase and 0.1 unit alkaline phosphatase were added and the reaction was continued for another 6 h. The reaction mixture was terminated by heating for 20 s at 110 °C to precipitate protein and then spun at 12 000 min^{-1} for 2 min to remove precipitate. The product [1′-^{3}H]NGD^+ was purified by injection of 500 μL onto a preparative C-18 column eluted with 50 mM ammonium acetate, pH 5.0. Eluted fractions of [1′-^{3}H]NGD^+ were lyophilized and were compared with authentic NGD^+ (Sigma) to verify purity. [8-^{3}H]NGD^+ was synthesized as above by incubating [8-^{3}H]-GTP with NMN^+ and coupling with NAD^+ pyrophosphorylase. After 12 h of coupling as above, the product [8-^{3}H]NGD^+ was purified. The isolated [8-^{3}H]NGD^+ was incubated in the presence of 20 mM [carbonyl-^{14}C]nicotinamide in 50 mM potassium phosphate pH 7.5. CD38 was added to a concentration of 0.05 μM, and the reaction monitored for incorporation of ^{14}C into NGD^+ by HPLC and scintillation counting. After the specific activity of ^{14}C in NGD^+ reached a plateau, the reaction was terminated by heating to 110 °C for 1 min and the reaction spun for 2 min to precipitate protein. The reaction was injected onto an HPLC column and the [8-^{3}H, carbonyl-^{14}C]NGD^+ purified as above. Specific activity of [8-^{3}H, carbonyl-^{14}C]NGD^+ was determined to be 30 000 cpm /nmol,^{3}H cpm /^{14}C cpm = 0.58

Kinetic Study of NMN^+ Hydrolysis by CD38. The desired concentrations of NMN^+ in 50 mM potassium phosphate pH 7.5 were prepared to volumes of 200 μL and equilibrated at 37 °C; 1 μL of 380 nM CD38 was added to start reactions.

Aliquots were taken at 30 s time intervals and quenched with a 10 vol % solution of 25% TCA. Assay was done by HPLC 95:5 A/B (A, 50 mM ammonium acetate, pH 5.0; B, 50% MeOH, 50% H_2O) on a Waters C-18 column to determine the amount of NMN^+ unreacted and the amount of nicotinamide formed. Plots of product formed vs time were used to determine initial reaction rates. A plot of NMN^+ concentration vs rate was fit using the program Kaleidograph to obtain the Michaelis parameters.

Enzymatic Assay of 7-Deaza-NHD$^+$and NHD$^+$. Solutions of 7-deaza NHD^+ and NHD^+ from 10 to 400 μM in 100 μL of 50 mM potassium phosphate pH 7.5 were equilibrated at 37 °C. 5 μL of CD38 (830 nM) was added to start each reaction. Aliquots (20 μL) of the reaction were taken at 30 s intervals and quenched with a 10 vol % solution of 25% TCA. Injection of samples onto a Waters C-18 column eluted with a 98:2 A/B (A, 50 mM ammonium acetate; B, 50% MeOH, 50% H_2O) at 2.0 mL/min permitted quantitation of the reaction components. Product formed vs time was plotted to determine initial reaction rates. The rates were plotted against substrate concentration and fit with Kaleidograph to a Michaelis curve to determine values for k_{cat} and K_m. NGD^+ at saturating concentrations (>50 μM) was run as a control.

Methanolysis of cADPR and NAD$^+$ by CD38. Solutions of 500 μM NAD^+ and 300 μM cADPR in 50 mM potassium phosphate pH 7.5 containing MeOH concentrations of 0.5, 1.0, and 2.0 M were prepared in volumes of 100−130 μL. CD38 was added (5.0 μL of 1.6 μM) to start the reaction and samples were taken to approximately 80% completion of reaction as determined by HPLC 96:4 A/B (A, 50 mM ammonium acetate, pH 5.0; B, 50% MeOH, 50% H_2O). The amounts of ADPR and α- and β-methoxy-ADPR were quantitated by HPLC peak area measurements. A control reaction without enzyme was used for each substrate in MeOH /H_2O 10:90 at pH 7.5 in 50 mM potassium phosphate buffer. Ratios of methoxy ethers to ADPR were determined by the ratio of peak areas. Peak areas were also used to determine the total amount of products formed of each species. Each reaction condition was plotted as follows: $R_{M/H}$ ($R_{M/H}$ = moles of methanolysis product/moles of hydrolysis product) vs MeOH concentration. Relative nucleophilicity was calculated by the equation RN = $R_{M/H}$ /([MeOH]/[H_2O]) where [H_2O] ≈ 55 M.

Stopped-Flow Studies of NGD$^+$ Cyclization. Fluorescence spectroscopy experiments were performed using a stopped-flow spectrophotometer fitted with dual syringe mounts and each contributing approximately 20 μL to give the total reaction volume of 40 μL. To the first syringe was added a CD38 solution of 4.0 or 8.0 μM in 50 mM acetate and 100 mM NaCl at pH 5.0. The other syringe contained 15 μM or 75 μM NGD^+ in 50 mM potassium phosphate pH 7.5. Excitation wavelength was 300 nm and emission intensity was observed using a 360-nm cutoff filter. Data were collected at time resolutions to 0.25 ms. The dead time on the instrument is <2.0 ms. Data were collected on disk and plotted and analyzed using Kaleidograph fits to a curve defined by: $E(t) = E_1 \exp(-k_1 t) + E_2 \exp(-k_2 t) + E_3 t + E_4$

Rapid-Quench Studies of NGD$^+$ Reaction with CD38. Concentrated enzyme CD38 in 50 mM acetate and 100 mM NaCl at pH 5.0 was placed into one syringe of a dual syringe rapid-mix rapid-quench instrument at 37 °C. To the other syringe was added [8-^{3}H, carbonyl-^{14}C]NGD^+ in 50 mM potassium phosphate pH 7.5 at either 18 or 72 μM, respectively. The reaction was quenched by a 20% TCA solution placed into the quench syringe. The quenched solutions were collected in eppendorf tubes and immediately placed on dry ice. The reaction times were varied from 1.8 ms to 305 ms in typical reactions. The collected solutions were thawed, spun at 12 000 min^{-1} to precipitate protein, and injected onto a Waters C-18 column eluted with 98:2 A/B (A, 50 mM ammonium acetate, pH 5.0; B, 50% MeOH, 50% H_2O). cGDPR, GDPR, NGD^+, and nicotinamide peaks were collected. The radioactive peaks (1.0 mL) were mixed with 9.0 mL of scintillation fluid to count the radioactivity. A blank and a ^{3}H standard were counted in order to determine background and counting efficiency. Plots of radioactivity and product vs time were generated and fit with the program Kaleidograph to a curve defined by:

$$P(t) = P_1 + P_2 \exp(-k_1 t) + P_3 t$$

Pulse-Chase Analysis of NGD$^+$ Reaction with CD38. The mixing syringes of a rapid-quench instrument were loaded with concentrated CD38 in 50 mM acetate and 100 mM NaCl at pH 5.0 and [1′-^{3}H]NGD^+ in 50 mM potassium phosphate pH 7.5, and the chase syringe was loaded with 50-fold excess NAD^+ in 50 mM potassium phosphate pH 7.5. Initial reaction time to chase was set to 7.5 ms, and a delay was inserted after chase of variable times 0−400 ms prior to an ejection pulse into a microcentrifuge tube containing 50% TCA to give the final quench of 10% TCA. For the zero-time point the quench was 30% TCA loaded to the quench (chase) syringe. The quenched reaction mixtures were injected onto a C-18 column and assayed as described above. The data were plotted against total reaction time for all products formed including nicotinamide. Commitment was determined by the relation C_f = (total moles of product from NGD^+ − moles of product at 7.5 ms)/(moles of enzyme − moles of product at 7.5 ms).

Nicotinamide Exchange Reaction. Solutions (100 μL) of 50 μM NGD^+ in 25 mM K_2HPO_4 pH 7.5 were equilibrated at 37 °C. Solutions included concentrations of nicotinamide from 1.0 to 16.0 mM with a specific radioactivity of 1 mCi /20 μmol. Reactions were initiated by addition of 5 μL of CD38 enzyme (0.40 μM) to a final concentration of 20 nM. Reactions were aliquoted in 20-μL volume at 30-s time intervals and quenched by addition of 2 μL of 25% TCA. Each sample was analyzed by injection onto a Waters C-18 HPLC column eluted with 97:3 A/B (A, 50 mM ammonium acetate, pH 5.0; B, 50% H_2O, 50% MeOH) to separate the reaction components. Integration of peak areas quantitated cGDPribose (5.4 min), GDPR (6.15 min), NGD^+ (7.8 min), and nicotinamide (15.4 min). The NGD^+ and nicotinamide peaks were collected and combined with 1.0 mL of eluant to 9.0 mL of scintillation fluid. Radioactivity was counted with a scintillation counter. A blank and a ^{14}C standard were run to determine the background and counting efficiency. The counts in each NGD^+ sample were subtracted against background to obtain total counts. Nicotinamide counts were similarly quantitated. The amount of nicotinamide incorporated vs time at each concentration was plotted as a function of time to obtain the initial rate of exchange. The rate of exchange was plotted against the nicotinamide

concentration and fit to a Michaelis curve using the program Kaleidagraph. A Dixon plot could also be derived by plotting the reciprocal of the rates of NGD^+ reaction to cGDPR and GDPR vs nicotinamide concentration.

Kinetics of Nicotinamide Inhibition of NGD^+ Cyclization and Hydrolysis (HPLC Method). Solutions of NGD^+ ranging in concentration from 20 to 200 μM containing different concentrations of nicotinamide (0, 1.0, 5.0, and 7.5 mM) in a volume of 100 μL of 50 mM potassium phosphate pH 7.5 were equilibrated to 37 °C. CD38 (5 μL of concentration 400 nM) was added to initiate the reaction. Aliquots in 20-μL amounts were taken at 30-s time points and quenched by addition of 2 μL of 25% TCA. Aliquots were injected under identical conditions to those above and areas of peaks quantitated to obtain amounts of cGDPR, GDPR, and NGD^+ present in each sample. The products formed (GDPR and cGDPR) were plotted vs time to a yield initial rate curves. Double reciprocal plots of $1/v$ vs $1/S$ for the different inhibitor concentrations were used to fit the data as straight lines. K_i values were obtained from the equation $E_0/v = 1/k_{cat}(1 + [I]/K_{ii}) + K_m/k_{cat}(1 + [I]/K_{is})$.

Fluorescence Study of Nicotinamide Inhibition of NGD^+ Cyclization (Stopped-Flow Method). Solutions containing 2, 4, 10, 20, and 50 μM NGD^+ in 50 mM potassium phosphate pH 7.5 were made to contain nicotinamide concentrations of 0, 5, 7.5, and 15 mM. Exact NGD^+ concentrations (0 mM nicotinamide) were determined at pH 7.5 by 253-nm absorbance using a value of ϵ_{max} of 17 750 M^{-1} cm^{-1}. To one syringe was added the desired NGD^+ and nicotinamide solution; to the other was added 100 nM CD38 in 50 mM potassium phosphate pH 7.5. Initial reaction rates were obtained in quadruplicate under the same reaction conditions. All reactions were performed at 36.8 ± 0.2 °C.

Reaction Coordinate Free-Energy Calculations. A reaction coordinate diagram (Scheme 6) fixed to free-energy levels was constructed using the reaction rates determined experimentally. The energies were calculated by the relation $\Delta G = -RT \ln (k_n h/kT)$ where k_n is the rate constant for a given step, h is Plancks constant, k is the Boltzmann constant, R is the ideal gas constant, and T is temperature in Kelvin. The potential energy wells for E•cGDPR and E•GDPR are undetermined and are approximated; thus the transition-state energy level of product dissociation is also approximate although the height of the energetic barrier is calculated in the forward direction. In addition, the energy level of the cGDPR product is calculated by literature values for bond strengths (*40*) assuming no strain energy and no entropy change vs the hydrolysis product for the cyclic geometry.

RESULTS

Methanolyses of NAD^+ and cADPR by CD38 and by Uncatalyzed Solvolysis. Methanol has been employed as an acceptor for ADP-ribosyl electrophiles to characterize the stereochemistry and character of the hydrolysis reaction of NAD^+ glycohydrolases (*41*−*43*). Stereochemical information for the hydrolytic product is lost by rapid equilibration of the epimeric forms. Products of alcoholysis reactions do not rapidly interconvert and can be used to determine the stereochemistry. The relative reactivity of MeOH and water were calculated as relative nucleophilicity, (RN =([methanolysis products]/[hydrolysis products])/([MeOH]/[H_2O]), to assess the electrophile selectivity. The anomeric configuration at the 1′-carbon and the extent of methanolysis and hydrolysis at different methanol concentrations were used to calculate the RN values for the reaction of CD38 with NAD^+ and cADPR (Figure 1). The slope of 0.20 indicates a relative nucleophilicity of 11 for MeOH/H_2O for solvolysis of both NAD^+ and cADPR by CD38. The slopes are linear and intersect at zero within experimental error. The curves for NAD^+ and cADPR solvolysis are the same for 0.5 to 2.0 M methanol. The α/β anomers for 1-methylribose products were produced at a ratio of 1:10 at all concentrations except at 2 M methanol with cADPR as a substrate, where the ratio of α/β was 1:20. The hydrolysis and methanolysis were also done in the absence of enzyme. The amount of methanolysis product increased linearly with methanol concentration, and the slope of the curve for NAD^+ was found to be 0.018 to obtain a relative nucleophilicity MeOH/H_2O of 1 (Figure 1). The same value has been reported for the solution methanolysis of NAD^+ (*43*). The uncatalyzed methanolysis products were formed in an approximate 1:1 ratio of α:β stereochemistry, consistent with the previous report (*43*).

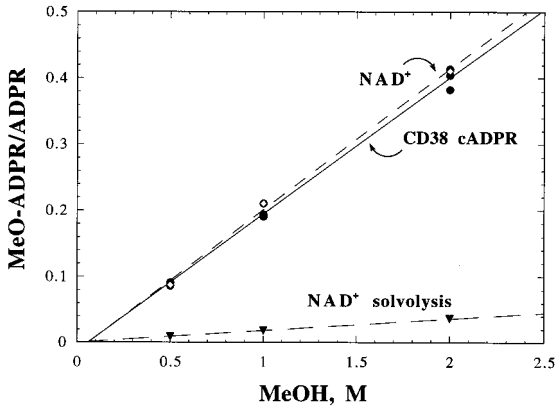

FIGURE 1: Competitive reaction of methanol and H_2O with NAD^+ and cADPR measured by HPLC. Plot of ratio of alcohol products/hydrolysis products vs concentration of methanol. The dashed line (open diamonds) is the solvolysis of NAD^+ mediated by CD38. The solid line (closed circles) is cADPR solvolysis mediated by CD38, and the dashed line (closed triangles) is the uncatalyzed solvolysis of NAD^+ in 50 mM phosphate buffer pH 7.5. Relative nucleophilicity for each line is calculated 55 × (slope) = RN. For each curve 11, 11 and 1 are the respective values for this parameter.

Scheme 1

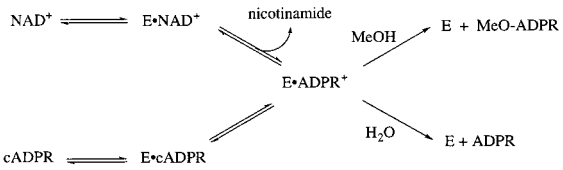

Conversion of both cADPR and NAD^+ to the same active site ADP-ribose electrophile unifies the reaction pathways leading to methanolysis and hydrolysis from both substrates (Scheme 1). The intermediate reacts with MeOH as both substrates reach an identical step along their reaction coordinates. This mechanism indicates that nicotinamide release precedes the methanolysis and hydrolysis of NAD^+. This mechanism has also been proposed to explain the activities of spleen NAD^+ glycohydrolases in their reaction with NGD^+ in the presence of methanol (*34*).

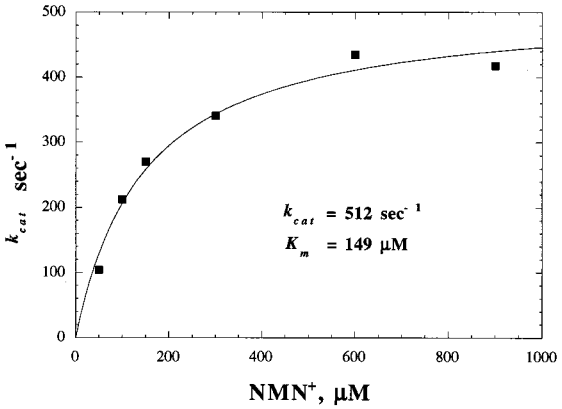

FIGURE 2: Dependence of initial reaction rate of NMN^+ hydrolysis vs NMN^+ concentration at 37 °C for the enzyme CD38. Solid squares represent experimentally measured rates as determined by HPLC. The solid line is the best fit to the Michaelis−Menten equation. Value of k_{cat} is 512 s^{-1} and K_m is 149 μM.

Scheme 2

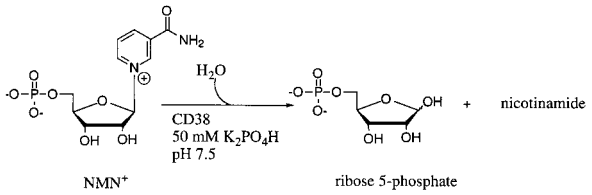

Table 1: Michaelis Parameters of Cyclizable and Noncyclizable Substrates for CD38[a]

substrate	k_{cat}, s^{-1}	K_m, μM
NAD^+ [b]	96 ± 5	16 ± 1
NMN^+	512 ± 32	149 ± 15
NHD^+ [b]	7.1 ± 2.2	23 ± 4
7-deaza-NHD^+ [c]	1.9 ± 0.3	3.1 ± 1.0

[a] All experiments performed at 37 °C by HPLC as indicated in Methods and Materials. Error is standard deviation multiple determinations. [b] Two product peaks detected; value represents the sum of cyclization and hydrolysis activities. [c] Only one product peak detected.

Reaction of NMN^+, 7-Deaza NHD^+, NHD^+, and NAD^+ with CD38. The mononucleotide NMN^+ is incapable of cyclization, but reacts rapidly with CD38 to form ribose 5-phosphate and nicotinamide (Scheme 2). The rate vs NMN^+ concentration yielded K_m and k_{cat} values of 149 μM and 512 s^{-1} per dimer (Figure 2). The k_{cat} for NMN^+ is greater by a factor of 5 than the value obtained for NAD^+ hydrolysis, while the K_m for NMN^+ is 10-fold greater than that for NAD^+ (Table 1).

The enzyme stabilizes the transition state of *N*-ribosyl hydrolysis without the requirement of a cyclic intermediate or the presence of AMP. The NAD^+ analogues NHD^+ and 7-deaza-NHD^+ were evaluated as substrates (Figure 3, Table 1). NHD^+ has been reported to be similar to NAD^+, forming predominantly IDPR with a minor cyclization product formed by ribosylation of the hypoxanthine ring at the 7-position (*44*). The deaza compound was used to determine if cyclization is required for hydrolysis of dinucleotides.

The k_{cat} value obtained for 7-deaza NHD^+ is 27% of the rate of the NHD^+ substrate, indicating that apparent transition-state stabilization is decreased by only 0.81 kcal/mol as a result of the inability of the 7-deaza compound to

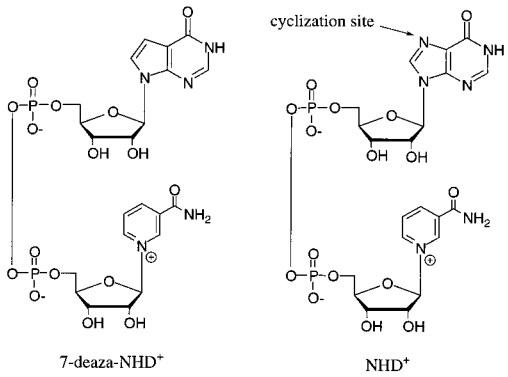

FIGURE 3: Chemical structures of 7-deaza-NHD^+ and NHD^+ and the site of cyclization on the purine ring of NHD^+ . The 7-deaza-NHD^+ lacks nucleophilicity at the 7-site.

cyclize. The substrates NMN^+ and 7-deaza-NHD^+ establish that hydrolysis and cyclization are two paths in a branched reaction coordinate. The K_m for 7-deaza NHD^+ is lower than that for the NHD^+ substrate, indicating that binding of the substrate is influenced by replacement of the N with a CH group (Table 1), or that the decrease in the catalytic rate reduces the K_m value.

Stopped-Flow Measurements of NGD^+ Cyclization: Steady State and Presteady State. Stopped-flow fluorescence measurements with NGD^+ indicated a phase of decreased emission prior to a burst in reaction rate for approximately 70 ms after which a linear steady-state rate was established (Figure 4B). The rapid burst is interpreted as on-enzyme production of cGDPR based on the fluorescence of the cyclic product. The steady-state rate is defined by a step following cGDPR formation and is related to product release. The burst phase has a rate of 52 s^{-1} compared to the steady-state rate of 7.5 s^{-1} per subunit. The duration of the initial emission decrease is NGD^+ dependent (Figure 4A,B). At 7.5 μM NGD^+ the duration of the decrease is approximately 20 ms, and at 37.5 μM NGD^+ the duration is approximately 8 ms. The signal is interpreted to be the binding of NGD^+ and was fit to a rate of 120 s^{-1} at 7.5 μM, for a bimolecular rate constant of 1.6×10^7 M^{-1} s^{-1}.

Rapid-Quench Studies of Pre-steady-State NGD^+ Cyclization. Rapid-mix−rapid-quench studies permit the direct measurement of nicotinamide, cGDPR, and GDPR to evaluate the microscopic rate constants. Mixing 9 μM [8-^{3}H,-carbonyl-^{14}C]NGD^+ with CD38 results in product formation at 1.8 ms, and approximately 80% of a single turnover occurs by 20 ms for a rate of 144 s^{-1} for NGD^+ based on the value of 1.6×10^7 M^{-1} s^{-1} from stopped-flow measurements. At 36 μM [8-^{3}H,carbonyl-^{14}C]NGD^+ and 6.5 μM CD38 the burst phase increased to 392 ± 75 s^{-1} (Figure 5A). This result establishes that the rate of enzyme-bound product formation is limited by the on-rate for substrate.

Analysis of the ratio of GDPR to cGDPR formed during the first turnover indicated that the product formation is primarily GDPR early in the reaction with increasing amounts of cGDPR in the first 50 ms (Figure 6). This result indicates an initial enzyme intermediate that yields GDPR upon quench. The decrease in the GDPR/cGDPR ratio over time provides a rate of 118 s^{-1} for decay of the intermediate. This value agrees reasonably with the value of 72 s^{-1} calculated for combined cGDPR and GDPR formation in the burst phase from stopped flow measurements.

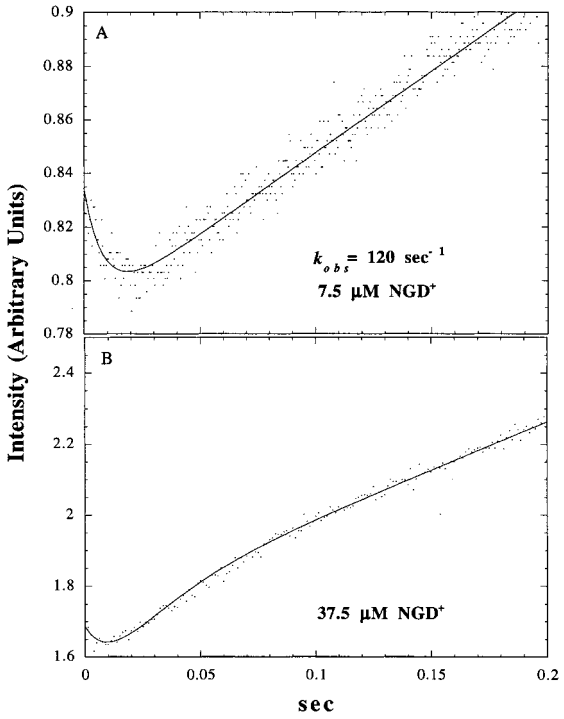

FIGURE 4: Stopped-flow fluorescence kinetic profile of CD38 reaction with NGD^+ at 37 °C. (A) Excitation wavelength is 300 nm. The output signal intensity was generated by passing the emission through a <360-nm cutoff filter. Fluorescence is shown in arbitrary units. Dots represent digitally recorded data. The top curve represents signal and curve fit for CD38 reaction with NGD^+ at 2 and 7.5 μM concentrations, respectively. Solid curve is best fit to the curve $E(t) = E_0 + E_1t + E_2 \exp(-k_{obs}t)$, $k_{obs} = 120$ s^{-1}. (B) Stopped-flow fluorescence kinetic profile of CD38 reaction with NGD^+ at 37 °C. Excitation wavelength is 300 nm. The output signal intensity was generated by passing the emission through a <360-nm cutoff filter. Fluorescence is shown in arbitrary units. Dots represent digitally recorded data. The top curve represents signal and curve fit for CD38 reaction with NGD^+ at 2 and 37.5 μM concentrations, respectively. Solid curve is best fit to the curve $E(t) = E_0 + E_1t + E_2 \exp(-k_{obs}t) + E_3 \exp(-k'_{obs}t)$, $k'_{obs} = 53$ s^{-1}.

Stoichiometry of Enzyme-Bound Product Formation. The magnitude of the burst is a measure of enzyme concentration when the rate of product formation pre-steady-state is much faster than rate limiting product release. The enzyme burst phase reaches only 1 mol of product per 2 mol of CD38 subunits before the onset of the steady-state rate, suggesting that two monomers are required to form one catalytic site (Figure 5B). Product formation on the enzyme of 392 s^{-1} exceeds the calculated product off-rate of 20 s^{-1} (dimer), so that the burst extrapolation is expected to give an intercept stoichiometry error of below 10%.

Pulse-Chase Analysis of the Pre-steady-State Reaction. Pulse-chase experiments provide the partition of enzyme-bound substrate between products and release to free substrate. [1′-^{3}H]NGD^+ was used as substrate and NAD^+ as the chase. Enzyme and [1′-^{3}H]NGD^+ were mixed (19 °C) to form the Michaelis complex and were diluted with excess NAD^+ at 7.5 ms. The time-dependent product formation following dilution by NAD^+ (Figure 7) gave a measure of the [1′-^{3}H]NGD^+ in the Michaelis complex that is committed to catalysis. The amount trapped is in excess of 70% per subunit. This value is greater than the theoretical maximum of 50% assuming one binding site per two subunits. The low number of total counts in the measurement introduces an error of ±35%. However, the result demonstrates that the forward reaction progress is fast relative to substrate dissociation, i.e., $k_3 \gg k_2$ (Scheme 3). The plateau of product counts indicates that the chase is effective

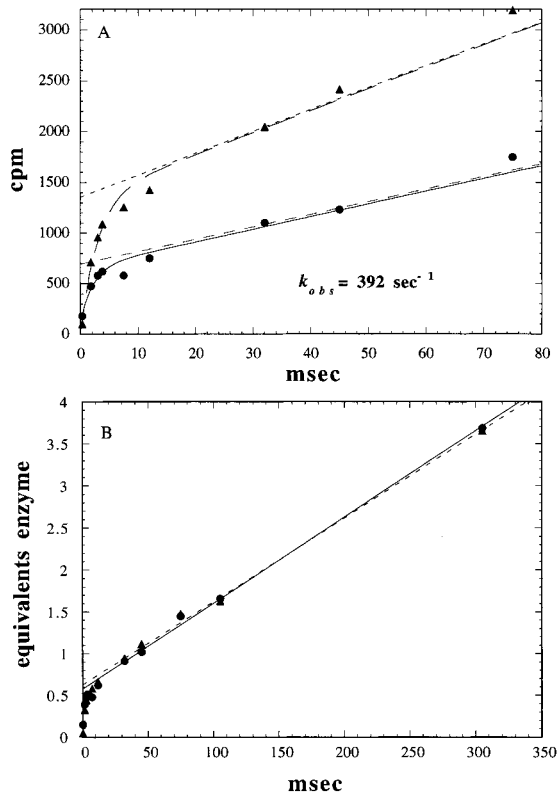

FIGURE 5: Formation of nicotinamide and combined GDPR + cGDPR by rapid-quench reaction of 36 μM [8-^{3}H, carbonyl-^{14}C]-NGD^+ with 6.5 μM CD38 at 37 °C. (A) Solid triangles represent nicotinamide formed at the times indicated; solid circles are combined GDPR and cGDPR formation measured in cpm. The solid curves represent best fits of the points to a curve of the type $y(t) = A \exp(-k_{obs}t) + Bt + C$. Top and bottom curves produced values of $k_{obs} = 339$ s^{-1} and $k_{obs} = 446$ s^{-1}. The average value obtained of k_{obs} is 392 ± 75 s^{-1}. (B) Formation of nicotinamide and combined GDPR + cGDPR by rapid-quench reaction of 36 μM [8-^{3}H, carbonyl-^{14}C]NGD^+ with 6.5 μM CD38 at 37 °C expressed as equivalents of enzyme. Solid triangles represent nicotinamide formed at the times indicated; solid circles are combined GDPR and cGDPR formation. The solid curves and dashed curves represent linear best fits of the points beyond 30 ms extrapolated to the *y*-axis. The *y*-axis intercept in both cases produces a value of 0.5.

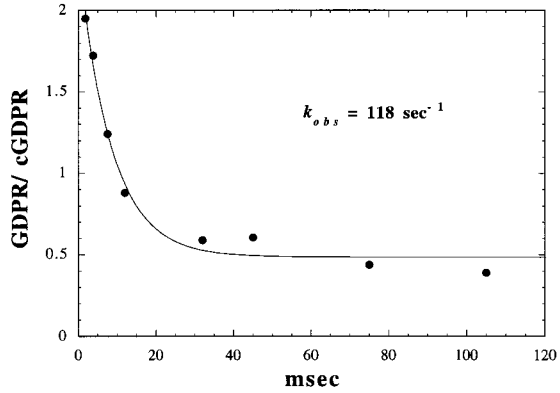

FIGURE 6: Decay of hydrolysis-to-cyclization ratio in the transient-phase reaction of 36 μM NGD^+ and 6.5 μM CD38 at 37 °C. The solid curve represents best fit to a curve of the type $y(t) = A \exp(-k_{obs}t) + B$, $k_{obs} = 118$ s^{-1}. The steady-state ratio is 0.38.

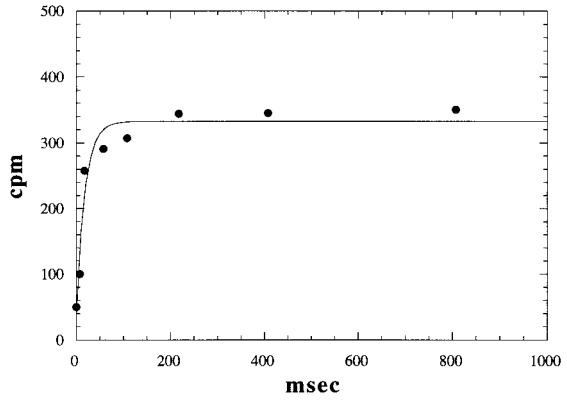

FIGURE 7: Pulse-chase analysis of reaction of [1′-^{3}H]NGD$^+$ and CD38. Time points represent time after initial mix of NGD$^+$ and CD38. Pulse time was 7.5 ms followed by the 50-fold dilution with NAD$^+$. The time point at 7.5 ms is the extent of reaction using a quench (TCA) at 7.5 ms. Following time points were quenched by TCA after the pulse was aged with NAD$^+$. Commitment is determined by C_f = [(moles of product formed from NGD$^+$) − (moles of product formed (7.5 ms))]/(moles of enzyme). The value obtained was 1.4. The solid curve represents best fit of the points to a curve of the type $y(t) = A - A\exp(-k_{obs}t) + B$, $k_{obs} = 60$ s^{-1}.

in dilution of labeled NGD$^+$. The results also indicate that the enzyme is saturated with NGD$^+$ at 7.5 ms and product formation has begun before the first acid quench occurs at 7.5 ms. The rate of product formation in the trapping behaves as a single exponential with a rate constant of 60 s^{-1} assigned to the forward reaction of NGD$^+$ to the enzyme-bound intermediate and nicotinamide. A similar experiment performed at 37 °C provided a rate constant in excess of 300 s^{-1} but could not accurately establish the rate due to the reaction rate exceeding the dead time of the instrument.

Exchange of Nicotinamide during Initial Reaction Rate. Nicotinamide exchange has been reported to be a significant feature of NAD$^+$ glycohydrolases including those from spleen (canine and bovine). Both CD38 and ADP-ribosyl cyclase exhibit this behavior (*11*, *16*). Exchange requires the sequential release of nicotinamide and rebinding followed by reaction with the enzyme-bound ADPR, consistent with a ping-pong mechanism. The sequential release of first product and rebinding of alternate first product prior to second product release provides an opportunity for the reaction to reverse to substrate, provided that the intermediate formed on the enzyme reacts reversibly. Since the $\Delta G°$ for nicotinamide hydrolysis is ca. −8.2 kcal/mol (*45*), exchange indicates stabilization of a high-energy form of ADPR bound as a reactive intermediate. Addition of radioactive nicotinamide makes it possible to measure the kinetic parameters of base exchange. The exchange process at 50 μM NGD$^+$ (excess of 10 times K_m) exhibits saturation kinetics vs nicotinamide and reaches saturation as predicted by Michaelis−Menten kinetics (Figure 8A). The k_{cat} for exchange is 117 s^{-1} and the K_m value for nicotinamide is 8.0 mM. The reciprocal rate of product formed varied linearly with the concentration of nicotinamide in a Dixon plot (Figure 8B). The result indicates that the forward and reverse reactions are joined by a common intermediate responsible for the ribosylating activity of the enzyme. High nicotinamide concentrations inhibit the forward reaction and activate the exchange reaction. The saturable maximum of the exchange establishes that nicotinamide is not a competitive inhibitor of NGD$^+$.

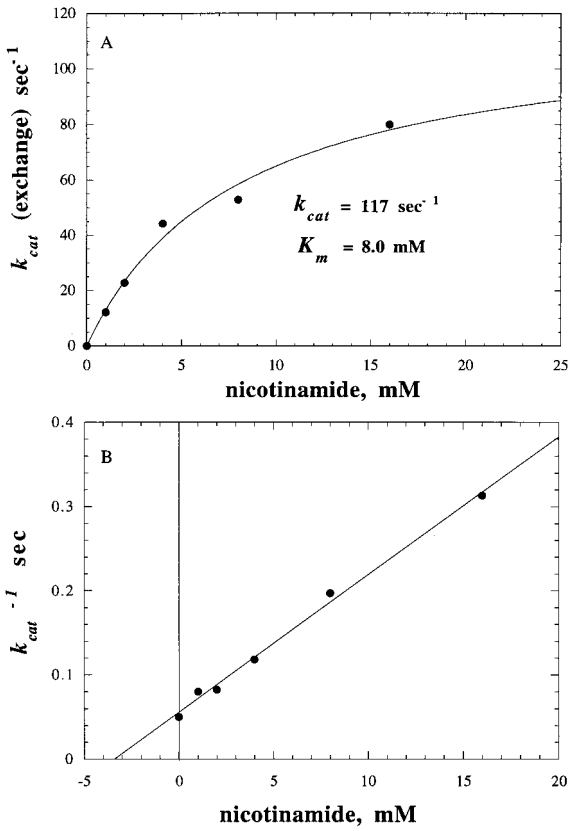

FIGURE 8: Panel A: Initial rate exchange kinetics of ^{14}C nicotinamide into NGD$^+$ as a function of ^{14}C nicotinamide concentration (0.02 μmol per μCi). Solid circles represent experimental points obtained for rates at 37 °C. The curve is the best fit to the Michaelis−Menten equation. Values of k_{cat} and K_m are 117 s^{-1} and 8.0 mM, respectively. NGD$^+$ concentration was near saturation at 50 μM. Panel B: Dixon plot of initial rates of NGD$^+$ hydrolysis and cyclization (combined) at 37 °C as a function of nicotinamide concentration as determined by HPLC. Concentration of NGD$^+$ in each experiment was 50 μM. Solid circles represent experimentally determined values. Solid curve is the best least-squares fit to a straight line. The highest level of inhibition measured is at greater than 2 × K_i showing that the inhibition remains linear even at high nicotinamide site saturation.

Inhibition of CD38 by Nicotinamide. Inhibition of CD38 by nicotinamide had been reported previously (*35*, *46*). Linear noncompetitive inhibition of the mixed variety was anticipated based on the mechanism of Scheme 3. The inhibition curves shown display both slope and intercept effects (Figure 9). K_i(intercept) was 7.1 ± 0.1 mM (7.0 mM HPLC); K_i(slope) was 1.4 ± 0.1 mM. The value of K_i(intercept) agrees well with the K_m of nicotinamide for the base exchange reaction.

DISCUSSION

Kinetic Mechanism of CD38. Two mechanisms proposed for CD38 represent distinct chemical pathways describing a "sequential intermediate mechanism" (SIM) and a "partition mechanism" (PM), respectively. Inherent to the SIM is the formation of a cyclic dinucleotide prior to any hydrolytic step. Inherent to the PM is a stabilized active site intermediate capable of behaving as a ribosylating electrophile. All the observed products and chemistry of the enzyme are presumed to traffic through this single reactive entity.

The SIM pathway has been criticized on kinetic grounds (*34*) and cannot function as a hydrolase with substrates

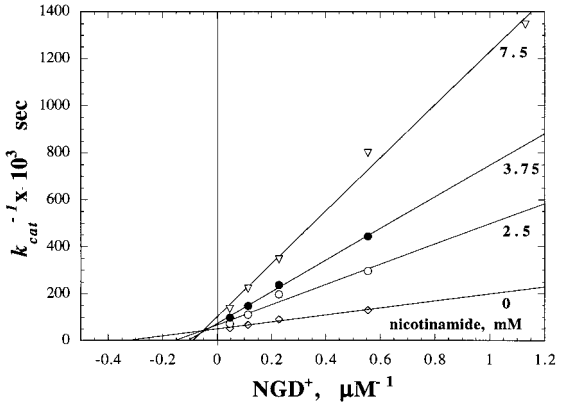

FIGURE 9: Inhibition of CD38 by nicotinamide. The ordinate is reciprocal initial rate determination of NGD^+ cyclization as determined by fluorescence spectroscopy. Nicotinamide concentrations are labeled. The abscissa is reciprocal NGD^+ concentration (μM). The data were fit to the equation for noncompetitive inhibition to give $K_{ii} = 7.2$ mM. $K_{is} = 1.4$ mM. Values are based upon best fit to the equation $E/v = K_m/k_{cat}(1 + [I]/K_{is}) + 1/k_{cat}(1 + [I]/K_{ii})$.

lacking the ability to cyclize. Two such substrates, 7-deaza-NHD^+ and NMN^+, were used in this study to eliminate the SIM mechanism. Previous work verified that the product of NHD^+ treated with CD38 was a combination of cIDPR and IDPR. cIDPR was found to be a substrate of the hydrolase. By removing the nitrogen from the 7-position, the hydrolase activity can be analyzed separate from the cyclization reaction. The hydrolase remains an active catalyst for 7-deaza-NHD^+ (k_{cat} values 1.9 s^{-1} vs 7.1 s^{-1}) when compared with the substrate NHD^+. The robust activity suggests that the hydrolase function of the enzyme is independent of cyclase activity. NMN^+ cannot cyclize, and its strong substrate properties also discount the SIM mechanism. NMN^+ is the first mononucleotide reported to be a substrate of CD38. Hydrolysis of NMN^+ by CD38 ($k_{cat} = 512$ s^{-1}) is five times faster than that of NAD^+ hydrolysis. This is the most active k_{cat} for any substrate of CD38. The lack of a cyclization along the hydrolytic pathway as exemplified by the hydrolysis of NMN^+ undermines the principles of the SIM model.

Support for the PM pathway requires evidence for a common intermediate to unite the production and hydrolysis of cADPR with the hydrolysis of NAD^+. If both cADPR and NAD^+ hydrolysis and cADPR formation proceed directly from a single intermediate product, distributions of methanolyses must be identical for these two substrates assuming the departure of nicotinamide prior to product formation on the enzyme. The results clearly satisfy this prediction. Both substrates give identical ratios of MeO-ADPR/ADPR at the three methanol concentrations studied as shown in Figure 1. The linear increase in MeO-ADPR/ADPR with methanol concentration indicates that the intermediate is stabilized and reacts with MeOH only after solvent equilibration with the active site. Retention of configuration in the methanolysis products is also consistent with the proposal that the intermediate responsible for hydrolysis of NAD^+ also generates cADPR, a product that also exhibits retention of stereochemistry relative to NAD^+. The presence of a significant α-stereochemical yield for methanolyses suggests that the reactive species is a stabilized oxo-carbenium ion at the active site, with the preferred route of attack to yield the β-anomer.

Table 2: Kinetic and Michaelis Parameters Based on Scheme 3 and Experimentally Determined Values[a]

parameter	equality of microscopic rates	experimental value
k_{cat} (hydrolysis)	$k_5'k_3/(k_3 + k_5')$[b]	5.3 ± 0.3 s^{-1}
k_{cat} (cyclization)	$k_5''k_3/(k_3 + k_5'')$[c]	15 ± 1.0 s^{-1}
k_{cat} (exchange)	$k_2k_3/(k_2 + k_3)$	118 ± 12 s^{-1} [d]
K_m (NGD)	$k_5(k_2 + k_3)/k_1(k_5 + k_3)$[e]	2.0 ± 0.5 μM
K_m (nicotinamide exchange)	$(k_5 + k_3)/k_4$	8.0 ± 0.5 mM
K_i (nicotinamide)	$(k_5 + k_3)/k_4$	7.1 ± 0.1 mM
C_f (commitment)	k_3/k_2	$k_3 \gg k_2$ ($1.4 \pm 0.5 = k_3/(k_3 + k_2)$)[c]

[a] All values were obtained at 37 °C except for C_f which was determined at 20 °C. Algebraic values for Michaelis constants were determined by the net rate-constant method of Cleland (*47*). [b] k_5' represents the rate constant for formation of the hydrolytic product. [c] k_5'' represents the rate constant for formation of the cyclized product. [d] Single determination, counting error was used to determine error. [e] $k_5 = k_5' + k_5''$, $k_5'/k_5'' = 0.38$.

Base Exchange, Nicotinamide Inhibition, and Obligate Release of Nicotinamide. Incubation of CD38, ADP-ribosyl cyclase, and spleen NAD^+ glycohydrolases with a dinucleotide such as NAD^+ and a pyridinium base (including nicotinamide) results in incorporation of the base with retention of stereochemistry (*11*, *16*, *33*, *41*, *45*). Work on the NAD^+ glycohydrolase from spleen provided an early example of this reaction in an isotope-exchange experiment (*45*). Nicotinamide with a ^{14}C label resulted in incorporation of the label into the initial substrate during catalysis. This behavior is typical of ping-pong mechanisms where a reactive intermediate is formed on the enzyme. Predictions for this mechanism include mixed noncompetitive inhibition of the forward reaction by nicotinamide and saturation kinetics for the exchange reaction. CD38 also conforms to this inhibition pattern. Equations which relate the exchange reaction and the product inhibition constant demonstrate the relationship K_m(exchange) = K_i(intercept). The K_m for the exchange reaction was 8.0 mM, in good agreement with the value of 7.2 mM K_i(intercept) obtained by inhibition studies. The linearity of the Dixon plot (Figure 8B) at high nicotinamide concentrations ($2 \times K_i$) indicates that nicotinamide dissociation from the enzyme occurs before the intermediate reacts.

The slope changes in the inhibition curves (Figure 9) can be explained by nicotinamide binding only to the stabilized oxocarbenium intermediate. There is no competitive behavior with NGD^+ binding at these concentrations. The lines for the double reciprocal plots at various nicotinamide concentrations are predicted to follow the behavior of the algebraic expression $E_0/v = K_m/k_{cat}[S](1 + k_2[I]/k_1K_mK_i)) + 1/k_{cat}(1 + [I]/K_i)$. The value of k_2 is 168 s^{-1} (Table 3, k_{cat}(exchange) = $k_2k_3/(k_2 + k_3)$) and that of k_1 of 1.6×10^7 M^{-1} s^{-1}. K_m was found to be 2 μM in several measurements. Using the relation $1/K_i$(slope) = $k_2/k_1K_mK_i$, the predicted value of K_i(slope) is 1.37 mM. The slopes of Figure 9 determine a K_i(slope) of 1.40 mM. Therefore the kinetic constants are internally consistent and support this mechanism.

Reaction Scheme and Determination of Steady-State Kinetic Parameters. Scheme 3 illustrates the minimal reaction pathway to describe the enzyme chemistry. Equations were derived for the behavior of the enzyme in steady-state, presteady state, exchange reactions, and inhibition.

Table 3: Experimentally Determined Microscopic Rate Constants Based upon Scheme 4[a]

rate constant	experimental value	method of calculation
k_1	$1.6 \pm 0.2 \times 10^7$ M^{-1} s^{-1}	calculated from rapid quench and stopped-flow method[b]
k_2	165 ± 45 s^{-1}	$k_{cat}(ex.) = k_2k_3/(k_2 + k_3)$[c] K_i(slope)
k_3	392 ± 75 s^{-1}	rapid quench measurements[a]
k_4	$6.71 \pm 2.7 \times 10^4$ M^{-1} s^{-1}	calculated from $(k_3 + k_5 + k_6)/k_4$[c]
k_5 (cyclization)	85.5 ± 8 s^{-1}	transient phase rate of decay hydrolysis/cyclization ratio[d]
k_6 (hydrolysis)	32.5 ± 3.5 s^{-1}	transient phase rate of decay hydrolysis/cyclization ratio[d]
k_7	20 ± 1.5 s^{-1}	steady-state rate[b]

[a] All values are for CD38 activity using NGD^+ as a substrate at 37 °C in 50 mM potassium phosphate pH 7.5. [b] Error reported is standard deviation from multiple determinations. [c] Error in calculation is based upon the total percent error of the experimentally determined parameters. [d] Single determination, based upon $k_6/k_5 = 0.38$, counting error was used to determine error.

Scheme 3

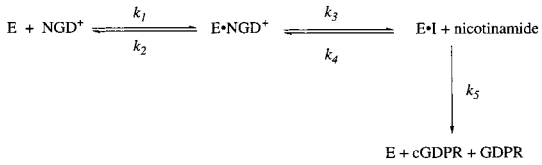

Values of parameters were calculated algebraically and are summarized in Table 2 using the Cleland method of net-rate constants (*47*). The K_m values for the exchange reaction are at saturating conditions of the dinucleotide substrate NGD^+.

Characterization of CD38 as a Functional Dimer. Burst kinetics were used to establish that CD38 behaves as a dimer in solution where each individual molecule contains a single active site per two subunits. The *y*-intercept for number of turnovers of the steady-state curve (Figure 5B) yields number of turnovers per monomer of enzyme. The value of the intercept is determined by the equation $y_{int} = E_0k_2^2/(k_2 + k_{cat})^2$ where k_2 is the burst rate and E_0 is the monomer concentration. Using a value of k_2 of 392 s^{-1} and 20 s^{-1} for k_{cat}, the inherent error is found to be no more than 10%. The intercept value obtained was 0.5 turnover per monomer.

The CD38 homologue *Aplysia* ADP-ribosyl cyclase has been crystallized and its structure solved to 2.4 Å resolution. The structure reveals that two monomers are joined in a dimeric interaction to form a deep tunnel created by facing clefts of the subunits (*28*). The tunnel has been suggested to be the active site of the enzyme with each subunit organized along a 2-fold axis to create the complete catalytic site (*28*). High homology of ADP-ribosyl cyclases with CD38 suggests that CD38 exists as a dimer as well. Model studies appear to confirm the reasonableness of this view (*28*). The data reported here support this view of the structure of the CD38 enzyme and by extension support the view that the activity of ADP-ribosyl cyclases is situated at a single active site composed from a dimer of subunits.

Derivation of Microscopic Rate Constants for the Mechanism of CD38: Evaluation of k_7-Off-Rate of Products. The steady-state and pre-steady-state rates permit numerical determinations of the individual rate constants including the rate constant k_7 for the release of products. Separate steps k_5 and k_6 are introduced for the chemical reaction of the ribosyl intermediate and k_7 for the product dissociation steps (Scheme 4).

Scheme 4

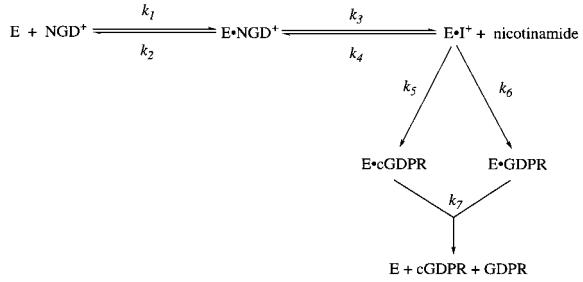

Stopped-flow experiments and rapid-quench studies indicate slow dissociation of product relative to product formation. With the assumption that $k_5 + k_6 \gg k_7$ (necessary for burst kinetics), then it is possible to approximate $k_7 = k_{cat}$ equivalent to a first-order rate constant $k_7 = 20$ s^{-1} for the product dissociation rate (*48*, *49*).

The Burst of Nicotinamide and cGDPR and GDPR Formed in Presteady State: Values of k_3, k_5, and k_6. The burst component can be fit to the equation $A + Bt + C \exp(-k_{obs}t) = P(t)$, where k_{obs} corresponds to the experimental rate constant of the observable burst phase (*48*, *49*). At near saturating NGD^+ the burst rate constant was found to be 392 ± 75 s^{-1}, while the predicted value was expected to be 576 s^{-1} if the binding of NGD^+ is rate limiting. The rates suggest that the burst phase is limited by the on-enzyme cleavage of the nicotinamide bond. This interpretation is reasonable with the expected value obtained for nicotinamide bond-breakage rate of 240 s^{-1} calculated from the value of 60 s^{-1} observed from pulse-chase studies at 19 °C.

Determination of the sum of the rate constants $k_5 + k_6$ from stopped-flow measurements at 37 °C gave a value of 72 s^{-1}. The value incorporates both hydrolysis and cyclization, and is 52 s^{-1} based upon cyclization alone. A more direct and more accurate determination of $k_5 + k_6$ was made by monitoring the ratio of hydrolysis to cyclization in the burst phase of rapid-quench experiments. Chemical quenching of the reaction decomposed all intermediates formed by nicotinamide bond cleavage and gave a high ratio of hydrolysis to cyclization. The decrease in this ratio to the steady-state value of 0.38 (k_6/k_5) provided a measurement of the decay of the intermediate to products. The rate constant for this process was found to be 118 s^{-1} and was assigned to be $k_5 + k_6$. Using 118 s^{-1} as the best determination of this sum permits determination of both $k_5 = 85$ s^{-1} and $k_6 = 33$ s^{-1}.

A caveat on the determination of both k_3 and $k_5 + k_6$ rests in the assumption that nicotinamide dissociation from the enzyme is fast, i.e., much faster than 118 s^{-1}. This assumption is supported by the observed rate for the exchange process of 117 s^{-1} and the equality $k_{cat}(exchange) = k_2k_3/(k_3 + k_2)$. Pulse-chase analysis indicates that $k_2 \ll k_3$ based upon a high measured commitment to catalysis of bound substrate. The determined exchange rate demands that k_2 be at least 117 s^{-1} and that k_3 be substantially greater than 117 s^{-1}. This result indicates that nicotinamide product dissociation must be substantially faster than 118 s^{-1} because

Scheme 5

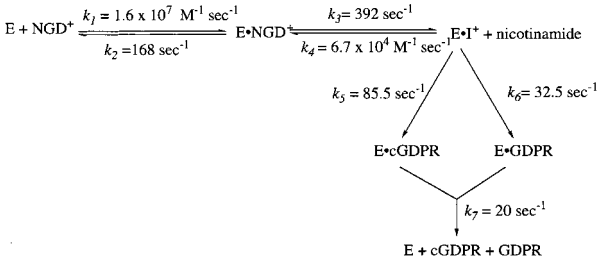

k_3 includes nicotinamide dissociation from the enzyme (Scheme 3).

Determination of k_4 and k_2. The value of k_4 could be calculated by the relationship $K_m = K_i = (k_3 + k_5 + k_6)/k_4$. Values for k_3 and $k_5 + k_6$ determined in the prior section permit the calculation of k_4. Using the average value of $K_m = K_i = 7.6 \pm 0.6$ mM obtained from inhibition studies and the exchange reaction, the value of k_4 could be calculated to be 6.71×10^4 M^{-1} s^{-1}. This value represents the rate constant for recombination of nicotinamide to the enzyme and reformation of substrate as shown in Scheme 4. k_2 was determined from the exchange study from $k_{cat} = k_2k_3/(k_2 + k_3)$. k_2 is determined to be 168 s^{-1}. k_2 can also be estimated from the slope behavior of the inhibition to be 165 s^{-1}. The value of k_2 predicts a forward commitment of bound substrate of 70% of bound NGD^+. This value is within the experimental error of the value determined by a pulse-chase experiment.

Evaluation of k_1: The Substrate On-Rate. The value of k_1 can be calculated directly from the value of k_{obs} for the decrease in emission in the stopped flow and from the rate of NGD^+ burst kinetics in rapid-quench experiments. Both experiments produce similar values for the magnitude of k_1 at 1.6×10^7 M^{-1} s^{-1}, which predicts a K_m of 1.3 μM in fair agreement with the experimental determination of $K_m = 2 \pm 0.5$ μM. The value of k_1 measured experimentally also depends on the contribution of k_2 and k_3 to its determination. The contribution of k_3 in the stopped flow will be minimal if the progress of the reaction forward does not alter fluorescence behavior of the bound chromophore. This assumption might be reasonable if the source of on-enzyme quenching is due to the guanine chromophore next to a tryptophan residue where nicotinamide bond breakage need not perturb the spatial behavior of guanine in the active site. Although k_2 is large compared to the measured magnitude of k_{obs}, forward commitment lessens the effect of dissociation on the measurement of the bimolecular association rate. In summary, there is good agreement of the experimental value of k_1 with the value of 1.4×10^7 M^{-1} s^{-1} determined by calculation using the other rate constants.

Reaction Profile. The reaction coordinate profile for the reaction of CD38 with NGD^+ has been resolved, and rate constants have been determined to create a complete set of microscopic rate constant set for CD38 reactions. This profile can be visualized as a reaction coordinate diagram (Scheme 6). The reaction mechanism and reaction coordinate are supported by results using noncyclizable substrates NMN^+ and 7-deaza-NHD^+. The mechanism of hydrolysis does not require cyclized intermediates. A stabilized intermediate consistent with the intermediate previously proposed to partition between cyclization and hydrolysis (*32*−*35*) is responsible for all the observed chemistry. This intermediate ($E•I^+$, Scheme 6) is a kinetically stabilized high-energy form of GDPR responsible for base-exchange, cyclization, and hydrolytic reaction pathways. Because these pathways are competitive, perturbation of conditions such as the increase of the concentration of one nucleophile over others can change the reactivity distribution of the intermediate to products.

The reaction coordinate includes two sequential chemical steps. The first step (k_3) is a rapid low-barrier breakage of the *N*-riboside bond to form an enzyme-stabilized ribosyl intermediate ($E•I^+$), likely an oxocarbenium ion and nicotinamide. Nicotinamide dissociates fast prior to subsequent chemistry. In the presence of high concentrations of base such as ^{14}C nicotinamide, the enzyme rebinds the base, and the reaction reverses to substrate (base-exchange reaction). In the absence of a competing base, the reaction continues forward to produce either cyclized or hydrolyzed product in a ratio of 1.0:0.38. Introduction of methanol gives 1-methoxy ribosides, confirming that the reactivity of the ribosyl electrophile is nonspecific. Some selectivity is observed between water and methanol to suggest that the transition state for the reaction of the nucleophile has significant bond order to the nucleophile, consistent with the reactivity of a stabilized cation in the active site. The formation of enzyme-

Scheme 6

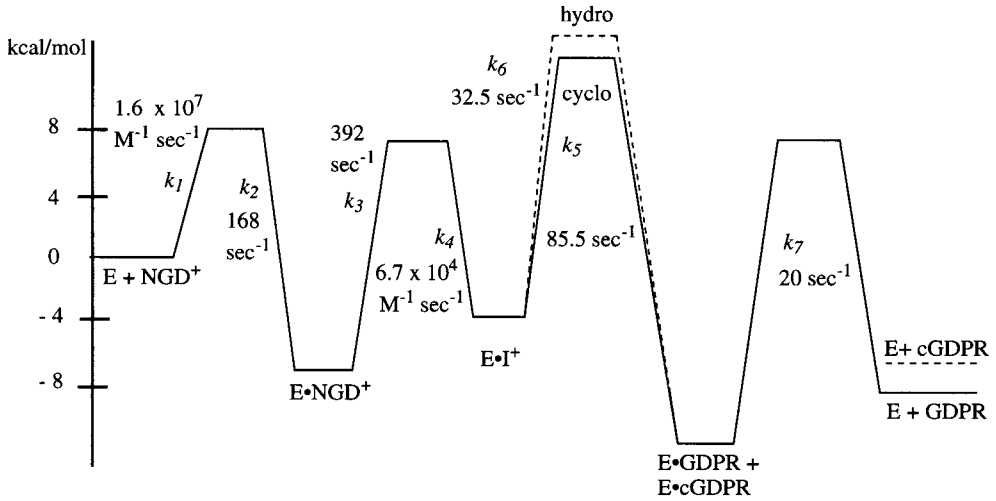

bound product ($k_5 + k_6$) is fast compared with product dissociation (k_7). The steady-state rate of CD38 appears to be limited by the nonchemical dissociation step of final product.

The coordinate presented in Scheme 6 suggests that forward commitment to catalysis would obscure isotope effects obtained from NGD^+ toward the cyclization reaction because of the slow off-rate (k_2) of bound NGD^+ relative to the first chemical step (k_3). Preliminary studies of NGD^+ cyclization studied by competition reaction of [1′-^{3}H]NGD^+ and [5′-^{14}C]NGD^+ confirm the absence of steady-state kinetic isotope effects for formation of cyclized product.[2]

The reaction mechanism presented offers an interpretation for the major chemical and kinetic steps of CD38. Efforts to further characterize the active site intermediate and to obtain KIEs for the chemical steps are in progress. Inhibitors of this enzyme based on the chemistry presented here should provide further insight into the in vivo significance of the enzyme function.

ACKNOWLEDGMENT

The authors thank Dr. Xiang-Yang Chen for his assistance in the adenosine kinase procedures and for purification of the enzyme.

REFERENCES

1. Mehta, K., Shahid, U., and Malavasi, F. (1996) *FASEB 10*, 1408−1417.
2. Jackson, D. G., and Bell, J. I. (1990) *J. Immunol. 144*, 7, 2811−2815.
3. Okamoto, H., Takasawa, S., Tohgo, A., Nata, K., Kato, I., and Noguchi, N. (1997) *Methods Enzymol. 280*, 306−317.
4. Nata, K., Takamura, T., Karasawa, T., Kumagai, T., Hashioka, W., Tohgo, A., Yonekura, H., Takasawa, S., Nakamura, S., and Okamoto, H. (1997) *Gene 186*, 285−292.
5. Kumagai, M., Coustan-Smith, E., Murray, D. J., Silvennoinen, O., Murti, K. G., Evans, W. E., Malavasi, F., and Camapana, D. (1995) *J. Exp. Med. 181*, 1101−1110.
6. Funaro, A Spagnoli, G. C., Ausiello, C. M., Allesio, M., Roggero, S., Delia, D., Zaccolo, M., and Malavasi, F. (1990) *J. Immunol. 145*, 2390−2396.
7. Deaglio, S., Dianzani, U., Horestein, A. L., Fernandez, J. E., Van Kooten, C., Bragardo, M., Garborino, G., Funaro, A., DiVirgilio, F., Banchereau, J., and Malavasi, F. (1996) *J. Immunol. 156*, 727−734.
8. Dianzani, U., Funaro, A., DiFranco, D., Garbarino, G., Bragardo, M., Redoglia, V., Buonfiglio, D., DeMonte, L. B., Pileri, A., and Malavasi, F. (1994) *J. Immunol. 153*, 952−959.
9. Hoshino, S., Kukimoto, I., Kontani, K., Kanda, Y., Malavasi, F., and Katada, T. (1997) *J. Immunol. 158*, 741−747.
10. Zocchi, E., Franco, L., Guida, L., Benatti, U., Bargellesi, A., Malavasi, F., Lee, H. C., and De Flora, A. (1993) *Biochem. Biophys. Res. Commun. 196*, 1459−1465.
11. Howard, M., Grimaldi, J. C., Bazan, J. F., Lund, F. E., Santos-Argumedo, L., Parkhouse, R. M., Walseth, T., and Lee, H. C. (1993) *Science 262*, 1056−1059.
12. Lund, F. E., Solvason, N. W., Cooke, M. P., Health, A. W., Grimaldi, J., Parkhouse, R. M., Goodnow, C. C., and Howard, M. C. (1995) *Eur. J. Immunol. 25*, 1338−1345.
13. Kontani, K., Kukimoto, I., Nishina, H., Hoshino, S., Hazeki, O., Kanaho, Y., and Katada, T. (1996) *J. Biol. Chem. 271*, 1534−1537.
14. States, D. J., Walseth, T. F., and Lee, H. C. (1992) *Trends Biochem. Sci. 17*, 495.
15. Gu, Q. M., and Sih, C. J. (1994) *J. Am. Chem. Soc. 116*, 7481−7486.
16. Lee, H. C., Galione, A., Walseth, T. F. (1994) *Vitamins and Hormones* (Litwack, G., Ed.) pp 199−258, Academic Press, Orlando, FL.
17. Lee, H. C., and Aarhus, R. (1991) *Cell Regul. 2*, 203−209.
18. Galione, A., White, A., Willmott, N., Turner, M., Potter, B. V. L., and Watson, S. P. (1993) *Nature 365*, 456−459.
19. DeFlora, A., Guida, L., Franco, L., Zocchi, E., Pestarino, M., Usai, C., Marchetti, C., Fedele, E., Fontana, G., and Raiteri, M. (1996) *Biochem. J. 328*, 665−672.
20. Willmott, N., Sethi, J. K., Walseth, T. F., Lee, H. C., White, A. M., and Galione, A. (1996) *J. Biol. Chem. 271*, 3699−3705.
21. Clementi, E., Riccio, M., Sciorati, C., Nistico, G., and Meldolesi, J. (1996) *J. Biol. Chem. 271*, 17739−17745.
22. Guse, A. H., Berg, I., da Silva, C., Potter, B., and Mayr, G. (1997) *J. Biol. Chem. 272*, 8546−8550.
23. Yamada, M., Mizuguchi, M., Otsuka, N., Ikeda, K., and Takahashi, H. (1997) *Brain Res. 756*, 52−60.
24. Mizuguchi, M., Otsuka, N., Sato, M., Ishii, Y., Kon, S., Yamada, M., Nishina, H., Katada, T., and Ikeda, K. (1995) *Brain Res. 697*, 235−240.
25. Koguma, T., Takasawa, S., Tohgo, A., Karasawa, T., Furuya, Y., Yonekura, H., and Okamoto, H. (1994) *Biochim. Biophys. Acta 1223*, 160−162.
26. Meszaros, L., Wrenn, R. W., and Varadi, G. (1997) *Biochem. Biophys. Res. Commun. 234*, 252−256.
27. Chini, E., and Dousa, T. P. (1995) *Biochem. Biophys. Res. Commun. 209*, 167−174.
28. Prasad, G., McRee, D., Stura, E., Levitt, D., Lee, H. C., Stout, and C. D. (1996) *Nature Struct. Biol. 3*, 957−964.
29. Fryxell, K. B., O'Donaghue, K., Graeff, R. M., Lee, H. C., and Branton, W. D. (1995) *Prot. Expr. Purif. 6*, 329−336.
30. Munshi, C. B., Fryxell, K. B., Lee, H. C., and Branton, W. D. (1997) *Methods Enzymol. 280*, 318−330.
31. Graeff, R. M., Walseth, T. F., Fryxell, K., Branton, W. D., and Lee, H. C. (1994) *J. Biol. Chem. 269*, 30260−30267.
32. Jacobson, M. K., Coyle, D. L., Vu, C. Q., Kim, H., and Jacobson, E. (1997) *Methods Enzymol. 280*, 265−274.
33. Kim, H., Jacobsen, E. L., and Jacobson, M. K. (1993) *Science* 261, 1330−1333.
34. Muller-Steffner, H. M., Augustin, A., and Schuber, F. (1996) *J. Biol. Chem. 271*, 23967−23972.
35. Berthelier, V., Tixier, J. M., Muller-Steffner, H., Schuber, F., and Deterre, P. (1998) *Biochem. J. 330*, 1383−1390.
36. Merkler, D. J., and Schramm V. L. (1987) *Anal. Biochem. 167*, 148−153.
37. Walseth, T. F., Aarhus, R., Gurnack, M. E., Wong, L., Breitinger, H. A., Gee, K. R., and Lee, H. C. (1997) *Methods Enzymol. 280*, 294−305.
38. Prescott, M., and McLennan, A. G. (1990) *Anal. Biochem. 184*, 330.
39. Rising, K. A., and Schramm, V. L. (1994) *J. Am. Chem. Soc. 116*, 6531−6536.
40. Section 9 (1994) in *Handbook of Chemistry and Physics*, 75th Ed. (Lide, D. R., Ed.) pp 69−73, CRC Press, Boca Raton, FL.
41. Schuber, F., Travo, P., and Pascal, M. (1976) *Eur. J. Biochem. 69*, 593−602.
42. Pascal, M., and Schuber, F. (1976) *FEBS Lett. 66*, 107−109.
43. Tarnus, C., Muller, H. M., and Schuber, F. (1988) *Bioorg. Chem. 16*, 38−51.
44. Graeff, R. M., Walseth, T. F., Hill, H. K., and Lee, H. C. (1996) *Biochemistry. 35*, 379−386.
45. Zatman, L. J., Kaplan, N. O., and Colowick, S. P. (1953) *J. Biol. Chem. 200*, 197−212.
46. Inageda, K., Takahashi, K., Tokita, K., Nishina, H., Kahano, Y., Kukimoto, I., Kontani, K., Hoshino, S., and Katada, T. (1995) *J. Biochem. 117*, 125−131.
47. Cleland, W. W. (1975) *Biochemistry 14*, 3220−3224.
48. Ouellet, L., and Laidler, K. J. (1956) *Can. J. Chem. 34*, 146.
49. Ouellet, L., and Stewart, J. A. (1959) *Can J. Chem. 37*, 737.

[2] Sauve, A. A., and Schramm, V. L., unpublished results.

BI981248S